BIOCHEMISTRY
including biophysical chemistry & molecular biology

Article

pubs.acs.org/biochemistry

Dimerization-Induced Folding of MST1 SARAH and the Influence of the Intrinsically Unstructured Inhibitory Domain: Low Thermodynamic Stability of Monomer

Diana Constantinescu Aruxandei,[†] Cihan Makbul,[†] Agne Koturenkiene, Maik-Borris Lüdemann, and Christian Herrmann*

Department of Physical Chemistry I, Ruhr University Bochum, Universitätsstrasse 150, 44780 Bochum, Germany

Supporting Information

ABSTRACT: The serine/threonine mammalian sterile 20-like kinase (MST1) is involved in promotion of caspase-dependent and independent apoptosis. Phosphorylation and oligomerization are required for its activation. The oligomerization domain, denoted as SARAH domain, forms an antiparallel coiled coil dimer, and it is important for both MST1 autophosphorylation and interactions with other proteins like the Rassf proteins containing also a SARAH domain. Here we show that the monomeric state of SARAH is thermodynamically unstable and that homodimerization is coupled with folding. Moreover, the influence of the inhibitory domain on SARAH stability and affinity is addressed. By investigating the thermal denaturation using differential scanning calorimetry and circular dichroism, we have found that the SARAH domain dissociates and unfolds cooperatively, without a stable intermediate monomeric state. Combining the data with information from isothermal titration calorimetry, a low thermodynamic stability of the monomeric species is obtained. Thus, it is proposed that the transition from MST1 SARAH homodimer to some specific heterodimer implies a non-native monomer intermediate. The inhibitory domain is found to be highly flexible and intrinsically unfolded, not only in isolation but also in the dimeric state of the inhibitory-SARAH construct. The existence of two caspase recognition motifs within the inhibitory domain suggests that its structural flexibility might be important for activation of MST1 during apoptosis. Moreover, the inhibitory domain increases the thermodynamic stability of the SARAH dimer and the homodimer affinity, while having almost no effect on the SARAH domain in the monomeric state. These results emphasize the importance of flexibility and binding-induced folding for specificity, affinity, and the capacity to switch from one state to another.

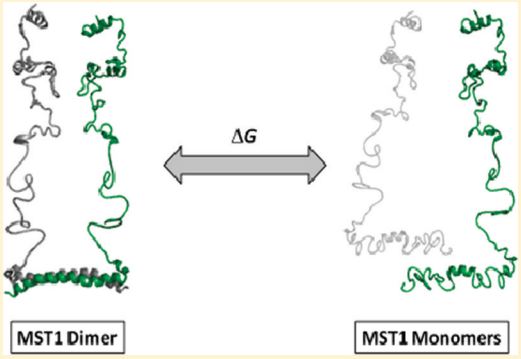

The mammalian sterile 20-like kinases (MST 1−4) belong to the germinal center kinase (GCK) subfamily of the mammalian Ste20-related protein kinases. MST1 and MST2 were found to be involved in apoptotic signaling pathways through activation of p38MAPK and JNK kinases,[1−3] whereas MST3 and MST4 specifically activate ERK mediated cell growth and transformation.[4,5] Several modulators or scaffold proteins of MST1/2 have been reported so far. Raf1 binds to MST2 and down-regulates its activity by inhibiting the dimerization. The Raf1−MST2 complex is dissociated by apoptotic stimuli like stress signals or activated Ras.[6−8] Death-associated protein 4 (DAP4) colocalizes MST1 with the proapoptotic nuclear protein p53 and augments MST1-induced apoptosis.[9]

MST1 is an ubiquitously expressed serine/threonine kinase, originally defined as kinase responsive to stress (Krs-2)[10] and detected in all tested human tissues and cell lines.[11] MST1 is activated by various proapoptotic stimuli and cellular stress,[1,10,12−14] and there are several studies describing the role of MST1 not only in human-derived cell lines but also in primary cells.[15−19] Its inactivation by promoter methylation was identified in 37% sarcomas.[20] Several substrates of MST1 kinase have been identified so far. For example, the human Salvador (hSav) enables MST1 to colocalize and phosphorylate the human large tumor suppressor (Lats1), a human orthologue of *Drosophila melanogaster* protein kinase Warts (Wts).[21] The caspase 3 cleaved MST1 phosphorylates nucleosomic histone H2B both in vertebrates and in *S. cerevisea*, leading to DNA fragmentation, chromatin condensation, and apoptosis.[22−24] Full length MST1 was recently found to phosphorylate the transcription factors FoxO in cytosol, inducing apoptosis in mammalian neurons[25] and also to inhibit and to be phosphorylated by Akt kinase.[26,27]

The human MST1 contains three domains: an N-terminal kinase domain (residues 1−330), an inhibitory domain (330−431), and an extreme C-terminal dimerization domain (431−487) known as SARAH domain. MST1 can be autoactivated by intermolecular cross-phosphorylation.[28] The region connecting the kinase domain to the oligomerization domain, known as the

Received: July 18, 2011
Revised: November 19, 2011
Published: November 23, 2011

inhibitory domain, was found to inhibit the kinase activity.[11] A disordered structure providing flexibility for domain motions was reported based on one-dimensional NMR and on circular dichroism spectroscopy, indicating 20% α-helix and 3% β-sheet content.[29] Several phosphorylation sites near a caspase 6/7-cleavage site (TMTD^{349}) close to this domain were recently found to be important in MST1 activity toward FoxO1 substrate. Thus, phosphorylation in the inhibitory region may lead to inhibition of caspase cleavage and retention of MST1 in the cytoplasm.[30] Phosphorylation found earlier to reside close to another caspase-cleavage site (DEMD^{326}) was reported to inhibit cleavage by caspase 3.[1]

The SARAH domain consists of the ultimate 57 C-terminal residues of MST1. It is responsible for homo- and hetero-oligomerization with other partners like the tumor suppressors Nore1 and Rassf1, mediating the Ras apoptotic signaling, although the exact mechanism remains unclear.[28,31,32] NMR structure analysis showed that the SARAH domain forms an antiparallel helical homodimer with a highly hydrophobic interface similar to coiled coil structures.[29] Each MST1 SARAH monomer consists of a long α-helix and a short N-terminal 3_{10}-helix folded toward the α-helix of the other molecule in the dimer (Figure 1). The kinked 3_{10}-helix would result in the proximity of the two kinase domains necessary for autophosphorylation. It was reported that the SARAH dimer represented a novel fold, as there were no close structural homologues[29] (PDB ID: 2JO8).

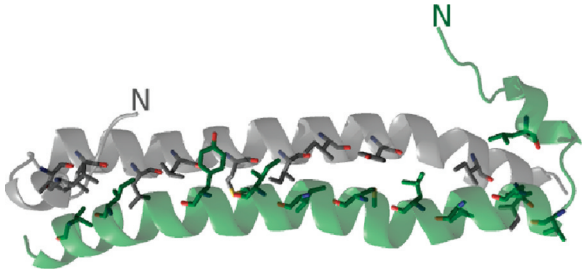

Figure 1. View of the MST1 SARAH dimer (NMR structure, PDB ID: 2JO8). The two chains are colored differently, and the hydrophobic residues that build contacts at the interface are shown as stick representation.

A detailed investigation on the kinetics of FoxO and histone H2B phosphorylation by MST1 and on the role of autophosphorylation and dimerization was reported.[30] The structural results of SARAH domain provided by Hwang et al.[29] and the recent structural analysis of the kinase domains of all MST members[33] brought some light into the possible mechanism of action of MST proteins. Nevertheless, this represents practically the only biophysical information related to MST1. In order to completely understand the processes involving these kinases, the interplay between structure, energetics, and dynamics should be elucidated. Thus, we investigated the thermal unfolding, stability, and affinity of MST1 SARAH domain and the influence of the inhibitory domain. This provided valuable information on the energetics of inter- and intramolecular interactions. We show that the SARAH domain is not stable as a monomer, while the inhibitory domain is found to represent an intrinsically disordered region (IDR). Moreover, the inhibitory domain brings additional thermodynamic stability to the dimeric state of the SARAH domain.

MATERIALS AND METHODS

Cloning, Expression, and Purification. Human MST1 SARAH (residues 437−487), inhibitory (330−431), and inhibitory-SARAH (330−487) DNA constructs were synthesized by PCR. The products were digested with *Bam*HI/*Eco*RI and inserted into the pGEX4T1 vector. The recombinant protein was expressed in *Escherichia coli* (BL21 strain) for 12 h at 25 °C after induction by 0.2 mM isopropyl-β-D-thiogalactoside (IPTG) at optical density, OD_{600}, of 0.7−0.8. The protein was subjected to two purification steps: a glutathion sepharose affinity chromatography using Tobacco Etch Virus (TEV) protease for proteolytic cleavage and a size-exclusion chromatography (on Superdex-75 column) as a final purification step and to exchange the buffer. Protein concentrations were determined by the Bradford method[34] and by UV absorption at 280 nm: ε_{280} = 6990 M^{-1} cm^{-1} (SARAH), ε_{280} = 6970 M^{-1} cm^{-1} (inhibitory), and ε_{280} = 15 470 M^{-1} cm^{-1} (inhibitory-SARAH).

Differential Scanning Calorimetry. Differential scanning calorimetry (DSC) was performed with a VP-DSC (MicroCal LLC, GE Healthcare, Northampton, MA), scanning the sample in the temperature range 20−100 °C. The buffer (20 mM sodium phosphate, 100 mM NaCl, pH 7.5) was filtered and degassed, and then the protein was diluted into the buffer from a highly concentrated stock solution. Evaluation of the thermodynamic data was done with the manufacturer's software (Microcal Origin 4.1). For each measurement, a reference scan of the buffer was subtracted from the experimental curve. The thermal profiles were normalized to the total protein concentration expressed as monomer, except where otherwise indicated. DSC scans were carried out as a function of scan rate, pH, or protein concentration. The calorimetric enthalpy, ΔH_{cal} (which is dependent on the protein concentration), was compared with the van't Hoff enthalpy, ΔH_{vH} (the enthalpy per cooperative unit, independent of the protein concentration) to establish the mechanism of thermal denaturation.

Circular Dichroism. The changes in secondary structure were probed by circular dichroism (CD) in the far-UV region (from 190 to 250 nm) on a JASCO J-715 spectropolarimeter. The protein concentration was varied between 0.5 and 35 μM, in 5 mM sodium phosphate, pH 7.5. The scans were performed in a 1 or 2 mm path length, rectangular quartz cuvette for concentrations higher than 5 μM and in a 5 or 10 mm cuvette for lower concentrations. For thermal denaturation, data points were taken at 222 nm, 2 or 5 °C intervals, with 1 min equilibration time at each temperature and a heating rate of 1 °C/min. For 10 μM MST1 SARAH concentration, the spectrum at each temperature was also collected. Spectra were recorded at a bandwidth of 1 nm and a scan rate of 50 nm/min. All measurements were an average of three consecutive scans. Buffer scans were accumulated under the same conditions and subtracted from the protein spectra before further analysis.

Isothermal Titration Calorimetry (ITC). ITC was used to measure the energetics and the K_D of MST1 dissociation. The measurements were performed with MicroCal ITC_{200}. The solution containing the appropriate concentration of protein was titrated from the syringe into the cell containing only buffer. The concentration in the syringe was more than 10 times higher than the expected dissociation constant (K_D). Thus, the protein in the syringe was predominantly dimeric, and it was diluted to concentrations where it was predom-

inantly monomeric. The injection volume was between 0.5 and 3 μL, and the time between the injections was 3 min. The buffers were filtered, degassed, and equilibrated at the desired temperature. The experimental points were fitted with a dimer dissociation model kindly provided by Prof. Alan Cooper.

Analytical Size-Exclusion Chromatography (SEC). The analytical SEC experiments were performed with a Superdex 75 16/60 column (GE Healthcare) after being calibrated with the following proteins: hGBP1 (69.3 kDa), BSA (66.3 kDa), ovalbumin (42.9 kDa), myoglobin (17.1 kDa), RNase A (13.7 kDa), RAF-RBD (9.2 kDa), and ubiquitin (8.6 kDa). All SEC experiments were performed with 100 μM protein in a buffer with 50 mM Tris (pH 7.4), 5 mM $MgCl_2$, 5 mM DTE, and 200 mM NaCl. 100 μL of each protein solution was applied to the SEC column. The measurements were repeated twice, and the apparent MWs were averaged.

Cross-Linking Experiments. The cross-linking experiments were performed on ice with 100 μM protein. A buffer containing 25 mM MES (pH 5) and 200 mM NaCl was used for the cross-linking experiments with 1-ethyl-3-(3-(dimethylamino)propyl)carbodiimide hydrochloride (EDC); 50 mM HEPES (pH 7) and 200 mM NaCl were used for α,ω-disuccinimidyl glutarate (DSG) cross-linking. Before adding EDC or DSG (Sigma-Aldrich, Hamburg/Germany), samples were taken from every protein solution (denominated as 0). The concentration of EDC of 1 mM at the beginning of the experiments was increased successively to 2 mM after 10 min, to 3 mM after 25 min, and to 4 mM after 55 min. The initial concentration of DSG was 0.25 mM and was successively increased to 0.75 mM after 20 min and to 1 mM after 40 min. The cross-linking reactions were stopped by mixing the samples with SDS sample buffer containing 10 mM β-mercaptoethanol (in case of EDC) or glycine (in case of DSG). Samples were taken after 5, 10, 15, 20, 30, 40, 60, and 80 min and analyzed by SDS-PAGE using 15% acrylamide gels.

Turbidity Assays. The turbidity assays were performed by means of a UV/vis photometer (Specord 200 Analytik Jena). All measurements were performed with 100 μg/mL protein in a buffer with 50 mM Tris (pH 7.4), 5 mM $MgCl_2$, 200 mM NaCl, and 5 mM DTE. First, the ODs of the protein solutions were measured at 20 °C. After that, the protein solutions were heated to 95 °C on a heat block for 10 min and immediately cooled to 20 °C on a prechilled metal block, before the ODs were measured again. Cytochrome *c* and lysozyme were purchased from Sigma-Aldrich.

Dynamic Light Scattering. The dynamic light scattering (DLS) measurements were performed using an ALV5000 DLS system (ALV GmbH Langen/Germany). Before measurements, the protein solutions (100 μM protein in 50 mM TrisHCl (pH 7.4), 5 mM $MgCl_2$, 5 mM DTE, and 200 mM NaCl) were filtered twice: first by a 40 μm and then by a 20 nm pore-size filter. The cuvettes were cleaned intensively with filtered buffer. DLS measurements were repeated 4−12 times, and the results were averaged. The autocorrelation functions were fitted with a single-exponential function using the software supplied by the manufacturer.

RESULTS

Thermal Denaturation of MST1 SARAH Domain. DSC is a powerful method for investigation of energetics of folding and structural architecture of proteins.[35] Thus, DSC was performed to study the mechanism and energetics of thermal denaturation of MST1 SARAH and to gain more information about the homodimerization of this domain. The thermal unfolding was highly reversible (more than 95%) when heating the protein up to 100 °C (Figure S1a). The reversibility was determined from the ratio between the calorimetric enthalpy, ΔH_{cal}, of the second scan and the one of the first scan.[36] Also, the protein underwent no exothermic irreversible aggregation. The absence of kinetically controlled processes during the transition was further supported by measuring the effect of the scan rate on the peak temperature (T_p), the temperature at which the heat capacity, C_p, has the maximum value. T_p was practically independent of the scan rate in the range 20−90 °C h^{-1} (Figure S1b). The same observation was made for the calorimetric enthalpy, ΔH_{cal}, and for the van't Hoff enthalpy, ΔH_{vH} (data not shown). All these observations demonstrate that reliable thermodynamic data can be extracted from the analysis of the DSC measurements.[37]

All scans performed under the conditions stated above gave asymmetric transitions, with T_m (the temperature at which the unfolding is 50%) lower than T_p, which suggests that the transition is accompanied by dissociation or/and that the unfolding mechanism involves several steps.[38] Indeed, the initial attempt to fit the thermogram by the simplest two-state model failed, the experimental transition being broader than the fit (Figure S2a). Further, by applying non-two-state model (including ΔH_{vH}), a deviation of the theoretical curve from the experimental one was evident (Figure S2b). Two sequential two-state transitions model gave better but still not appropriate fits (data not shown). Good fits were obtained either by applying the two-state dissociation model ($n = 2$) or by deconvoluting the transition into two sequential non-two-state transitions (Figures S2c and S2d, respectively).

For an oligomeric protein that undergoes thermal denaturation, the dependency on protein concentration can give valuable information on the possible dissociation/association during unfolding. If a transition involves dissociation of native species or aggregation of non-native ones during unfolding, a dependency of the melting temperature on the protein concentration should be observed, increasing in the first case and decreasing in the second one. By increasing the protein concentration 10 times, from 0.5 to 5 mg/mL, an increase of almost 5 °C in T_m was observed (Figure 2a and Table S1). Taking into account that the MST1 SARAH structure was found to be a constitutive dimer, the reciprocal of T_m was plotted against the natural logarithm of the total protein concentration, C_t (Figure 2b), and fitted using a derived van't Hoff equation, valid for a denaturation model involving dimer-to-monomer dissociation:[39]

$$\frac{1}{T_m} = \frac{R}{\Delta H_{conc}} \ln C_t + \frac{\Delta S_{conc}}{\Delta H_{conc}} \quad (1)$$

The linear dependency of T_m is an indication that the overall transition implies also dissociation. The enthalpy, ΔH_{conc}, and the entropy, ΔS_{conc}, of transition can be evaluated from the slope and the intercept with the ordinate, respectively. The enthalpy obtained by this method can be compared with ΔH_{vH} calculated from the individual heat capacity curves, according to either formula:[37]

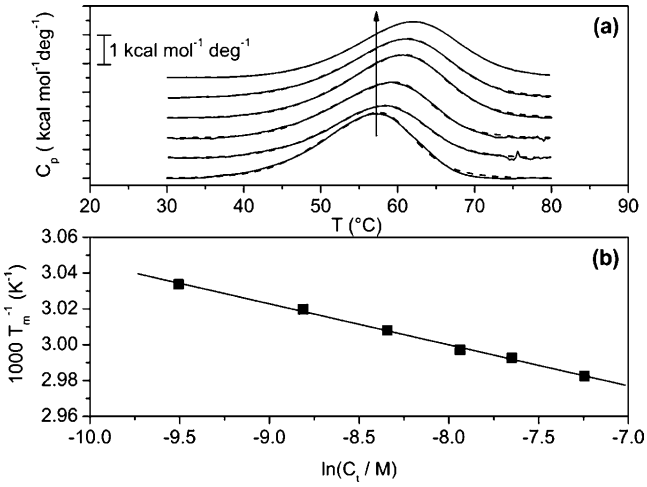

Figure 2. Protein concentration dependency of the thermal denaturation of MST1 SARAH probed by DSC. The concentration was varied between 74 and 740 μM (0.5−5 mg/mL); scan rate 60 °C h^{-1}. (a) DSC scans (solid lines) and the corresponding global sequential nontwo state fit (dashed lines). (b) T_m dependency on the total protein concentration, according to dimer-to-monomer dissociation model. The line represents the fit using eq 1.

$$\Delta H_{vH} = 2(n+1)RT_m^2\frac{\Delta C_{p,1/2}}{\Delta H_{cal}} \text{ or } \Delta H_{vH} = ART_p^2\frac{\Delta C_{max}}{\Delta H_{cal}} \quad (2)$$

where n is the number of subunits, $\Delta C_{p,1/2}$ is the molar excess heat capacity at T_m, and ΔC_{max} is the maximal molar excess heat capacity corresponding to T_p. The parameter A has the following values: 4 (n = 1 or $N_n \leftrightarrow U_n$ transition), 5.83 ($N_2 \leftrightarrow 2U$), 7.47 ($N_3 \leftrightarrow 3U$), 9.01 ($N_4 \leftrightarrow 4U$). R is the gas constant (1.987 cal mol^{-1} K^{-1}).

The processes involving dissociation can be either two-state (simultaneous unfolding and dissociation, no stable intermediates) or non-two-state (e.g., dissociation prior to unfolding).[40] Finally, if the right stoichiometry is applied for the calculation of enthalpies and the two-state model is considered valid, all three enthalpy values ΔH_{cal}, ΔH_{conc}, and ΔH_{vH} should be similar.[38]

The enthalpy value (ΔH_{conc}) obtained from Figure 2b is 87 ± 2 kcal (mol of cooperative dimer)$^{-1}$, and the entropy of unfolding (ΔS_{conc}) is 260 ± 10 cal (mol of cooperative dimer K)$^{-1}$. Considering a dimer-to-monomer transition (n = 2 or A = 5.83), an average value of 76 kcal (mol of cooperative dimer)$^{-1}$ for ΔH_{vH} was calculated from eq 2 (Table S2). Finally, by normalizing the thermograms to the total protein amount expressed as dimer concentration, an average total ΔH_{cal} of ≈70 kcal mol^{-1} is obtained (Tables S1 and S2). Although ΔH_{conc} was somewhat higher than the other two values, the dimer−monomer equilibrium appears to represent the adequate model. Considering the possibility of a higher oligomer formation, a trimer-to-monomer or a tetramer-to-monomer transition[39] gives ΔH_{conc} values much higher than the average ΔH_{cal} and the calculated ΔH_{vH} (Table S2).

The thermal denaturation was further investigated by far-UV circular dichroism to cover lower protein concentrations range. First, the effect of the protein concentration on the CD spectrum was investigated. As expected in case of monomers assembling to form a coiled coil, the ellipticity shifted to more negative values with increasing concentration (Figure 3a).

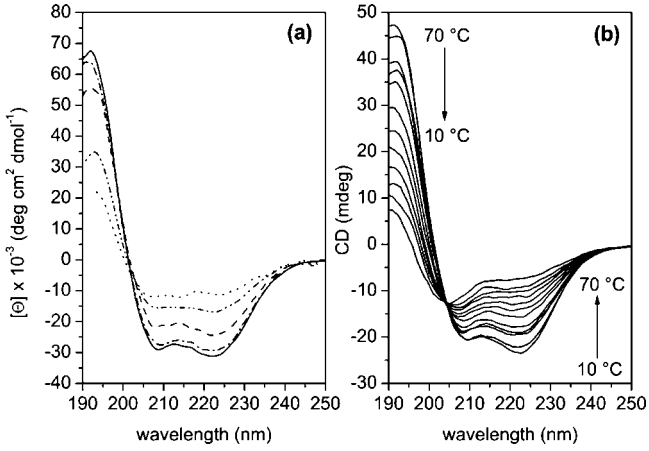

Figure 3. (a) Concentration dependency of the far-UV CD spectrum (mean residue ellipticity) for MST1 SARAH at 37 °C: 0.5 μM (dotted line), 1 μM (dashed dotted dotted line), 2.5 μM (dashed line), 15 μM (dashed dotted line), and 20 μM (solid line). (b) Far-UV CD spectra of 10 μM MST1 SARAH in 5 mM Na-phosphate buffer, pH 7.5, as a function of temperature.

Interestingly, also the ratio 222 nm/208 nm (which is supra-unitary for coiled coils) slightly increased (from 0.9 to 1.2), suggesting that more coiled coil α-helix was formed.[41]

Figure 3b displays the collected spectra for 10 μM MST1 SARAH at different temperatures from 10 to 70 °C. The spectrum at 10 °C is characteristic for a coiled coil like protein with two ellipticity minima, at 208 and 222 nm, the second one being more negative than the first (ratio 1.17). The ellipticity at 222 nm gets less negative with increasing temperature, and at a certain temperature, it also becomes less negative than the one at 208 nm. Apparently, an isodichroic point at 204 nm is observed. The thermal unfolding showed concentration dependency for all range of concentrations used in this study. The protein folded fraction was calculated from ellipticity at 222 nm measured for each temperature by the following formula:

$$f_N = \frac{\Theta_{obs} - (\Theta_U + m_U T)}{(\Theta_N + m_N T) - (\Theta_U + m_U T)} \quad (3)$$

where Θ_{obs} is the observed ellipticity, Θ_N and Θ_U represent the signal intensities of the native and the unfolded protein, respectively, and m_N and m_U are the pre- and post-transition slope, respectively.

Figure S3a shows typical curves for concentrations between 5 and 20 μM as a function of temperature, and the corresponding fits that were obtained by applying the following equation:

$$f_N = \frac{4K_F C_t + 1 - (8K_F C_t + 1)^{1/2}}{4K_F C_t} \quad (4)$$

dx.doi.org/10.1021/bi201110h | Biochemistry 2011, 50, 10990−11000

with

$$K_F = \exp\left[\frac{\Delta H_{vH}}{RT}\left(1 - \frac{T}{T_m}\right) - \frac{\Delta C_p}{RT}\left(T_m - T + T \ln\frac{T}{T_m}\right) - \ln C_t\right]$$

equation applied for two-state dimer−monomer transitions, where K_F is the folding constant and C_t is the total protein concentration, from where ΔH_{vH} and T_m are obtained.[42] The change in heat capacity (ΔC_p) was initially set to zero.[43] A value of 1.33 ± 0.15 kcal mol^{-1} deg^{-1} for ΔC_p was obtained by measuring DSC in buffer at different pH values. Interestingly, the fits of the CD denaturation curves using this value deviated from the experimental points (Figure S4). This can be an indication that the approximation of constant ΔC_p over the temperature range does not apply in case of MST1 SARAH or/and that other structural changes that cannot be detected by CD, but by DSC, take place.[41,44] In fact, this was observed even from the DSC thermogram as the heat capacity of the folded protein (pre-transition region) increased with temperature (Figure S1).

The same linear dependency of T_m as in the case of DSC was obtained (Figure S3b), but the van't Hoff enthalpies obtained from individual denaturation fits as well as from the linear dependency (eq 1) were a bit lower than the values obtained from DSC (with ≈5−10 kcal mol^{-1}). The data from DSC and CD were fitted together using eq 1, yielding ΔH_{conc} slightly different compared to ΔH_{conc} obtained from DSC only (73 vs 87 kcal mol^{-1}), but very close to the other DSC-derived ΔH values.

Affinity of MST1 SARAH Dimer and the Thermodynamics of Dissociation. From the dependency of ellipticity on the total protein concentration in the range 0.5−35 μM, an approximated K_D at 37 °C could be obtained. Thus, [Θ] at 222 nm was plotted against the protein concentration, and the experimental data points were fitted by the following equation (Figure S5a):

$$\Theta_{obs} = \Theta_D + (\Theta_N - \Theta_D)\frac{4C_t + K_D - \sqrt{K_D^2 + 8C_tK_D}}{4C_t} \quad (5)$$

where Θ_{obs} is the observed ellipticity at 222 nm, Θ_N and Θ_D represent the signal intensities of the native and of the dissociated protein, K_D is the dissociation constant, and C_t is the total protein concentration. The three parameters Θ_N, Θ_D, and K_D were let free to vary. The following values were obtained: Θ_N = −29 000 ± 360 deg cm^2 dmol^{-1}, Θ_D = −15 700 ± 2600 deg cm^2 dmol^{-1}, and K_D = 1.07 ± 0.7 μM. The corresponding ΔG of dissociation, ΔG_{diss}, is 8.65 ± 0.49 kcal mol^{-1}.

The affinity of MST1 dimer and the corresponding thermodynamics were further probed by ITC. The isotherm was fitted by a modified dimer dissociation model provided by Prof. Alan Cooper (Figure S5b). The K_D (0.9 ± 0.1 μM) is similar to the one obtained by CD. A corresponding ΔG_{diss} of 8.58 ± 0.07 kcal mol^{-1} is obtained. The dissociation is enthalpically unfavored (ΔH_{ass} = 16 ± 0.8 kcal mol^{-1}) and entropically favored ($T\Delta S_{ass}$ = 7.4 kcal mol^{-1}). An average ΔG_{diss} value of CD and ITC data of 8.62 ± 0.28 kcal mol^{-1} was used in subsequent analysis.

Influence of Inhibitory Domain on SARAH Stability and Affinity. The SARAH domain is connected to the kinase domain through a long (100 amino acids) region named the inhibitory domain. We were interested to see if this domain could have an influence on SARAH stability. Thus, the thermal denaturation as well as dissociation of MST1 inhibitory-SARAH construct were performed. The thermal stability of SARAH is increased by ∼10 °C (a similar result was obtained using CD, Figure S6b), and the domain unfolds after the inhibitory domain (which has a T_m around 40 °C) with an almost independent transition (Figure 4). The transition still displays protein concentration dependency and can be fitted to a two-state with dissociation model (data not shown). The resulting enthalpy change of the SARAH domain is similar to that for the isolated domain (72 ± 2 kcal mol^{-1}) while the entropy change is slightly lower (196 ± 10 cal mol^{-1} deg^{-1}).

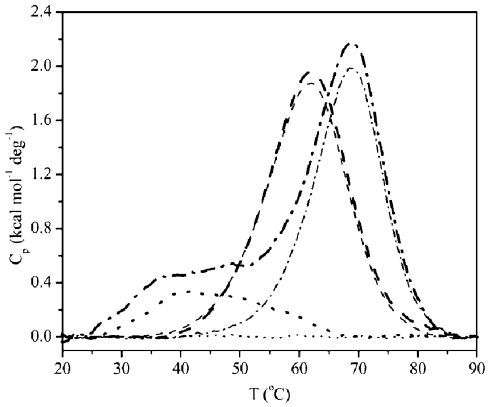

Figure 4. DSC thermograms of different MST1 constructs. MST1 inhibitory: first scan (thick dotted line), second scan (thin dotted line); MST1-SARAH: first scan (thick dashed line), second scan (thin dashed line); MST1 inhibitory-SARAH: first scan (thick dashed dotted line), second scan (thin dashed dotted line).

The MST1 inhibitory domain has a very small ΔH_{cal} (8 kcal mol^{-1}) which corresponds to less than a quarter of ΔH_{cal} of the SARAH domain (36 kcal mol^{-1}), although the molecular weight of MST1 inhibitory (11.84 kDa) is almost twice as large as that of the SARAH domain (6.7 kDa). The sum of ΔH_{cal}s of the inhibitory and SARAH domains as single recombinant domains (42 kcal mol^{-1}) is only slightly smaller than the overall ΔH_{cal} of MST1 inhibitory-SARAH (46 kcal mol^{-1}). MST1 Inhibitory has a melting temperature (T_m) of only 42 °C, a value which is 20 °C smaller than that of the SARAH domain. The second scan indicates that the unfolding of the MST1 inhibitory domain is irreversible (Figure 4, thin dotted line). The first scan for MST1 inhibitory-SARAH shows two transitions. The first transition can be attributed to the inhibitory domain and is irreversible; the second transition corresponds to the SARAH domain and is almost completely reversible (Figure 4).

The dissociation of MST1 inhibitory-SARAH could not be detected by ITC probably due to stronger interaction, even though the protein initial concentration was varied between 5 and 500 μM and the temperature between 20 and 40 °C. A K_D of 0.1 ± 0.07 μM at 37 °C was obtained from CD dilutions (Figure S7). This corresponds to a ΔG_{diss} of 10.14 ± 0.54 kcal mol^{-1}.

dx.doi.org/10.1021/bi201110h | Biochemistry 2011, 50, 10990−11000

Thermodynamic Stability of MST1 SARAH. As we are interested in the stability and affinity of the MST1 SARAH homodimer, we used the parameters obtained to calculate the Gibbs energy of unfolding at different temperatures around T_m (ΔG^0_U). This was calculated from the folded and unfolded fractions, considering a dimer−monomer two-states equilibrium.[42] Figure 5 shows the plot of ΔG^0_U for MST1 SARAH

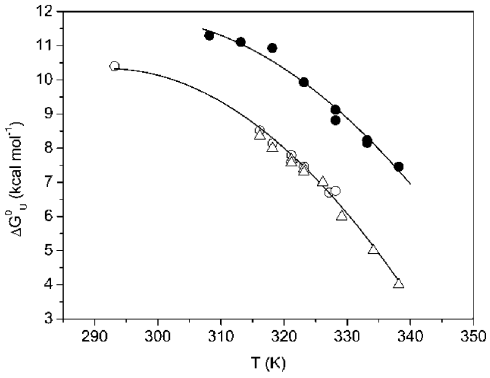

Figure 5. MST1 thermodynamic stability profiles determined from DSC (●) and CD (○) thermal denaturation for MST1 SARAH (△) and MST1 inhibitory-SARAH (□). The solid line represents the fit using eq 6 (see text).

(open symbols) as a function of temperature (ΔG^0_U at 293 K was obtained from urea denaturation) and the fit using the following equation:

$$\Delta G^0_U = \Delta H_1 - \left(\frac{T}{T_1}\right)(\Delta H_1 - \Delta G^0_{U1}) + \Delta C_p\left[T - T_1 + T\ln\left(\frac{T}{T_1}\right)\right] \quad (6)$$

where ΔG^0_{U1} is the unfolding free energy at a reference temperature T_1; the enthalpy of unfolding at T_1 (ΔH_1) and ΔC_p are obtained from the fit.

Moreover, a comparison between the free energy of unfolding and the free energy of dissociation (ΔG_{diss}) was performed at 37 °C in order to determine if the dissociation is accompanied by unfolding at physiologically relevant temperature.

The values calculated for different concentrations were similar and the fit (with ΔG^0_{U1} = 5.37 kcal mol^{-1} and T_1 = 333.15 K) gave similar ΔH_1 and ΔC_p as the ones obtained from direct analysis of thermal denaturation: 80 ± 2 kcal mol^{-1} and 1.56 ± 0.2 kcal mol^{-1} deg^{-1} (at 333.15 K), respectively. This validates the proposed model of simultaneous dissociation and unfolding in this temperature interval. At 37 °C, a value of 9.2 kcal mol^{-1} is obtained. At this temperature, the corresponding unfolding constant, K_U, from the folded dimer to the unfolded monomer is 0.3 μM. At 25 °C, on the other hand, the K_U is around 40 nM (±50%), almost 10 times less than at 37 °C. The MST1 SARAH dimer exhibits the maximum stability (ΔG^0_U = 10.6 kcal mol^{-1}) at around 13 °C.

Figure 5 also shows that the Gibbs energy of MST1 SARAH within the inhibitory-SARAH construct is higher with 2 kcal mol^{-1} than that of the domain in isolation. This indicates stabilizing interactions between SARAH and inhibitory domain. As the inhibitory domain in isolation displayed no significant change in ellipticity, the main thermal transition was considered as unfolding of SARAH (Figure S6a). As mentioned above, the T_m of SARAH unfolding increases by 10 °C. The fit of Gibbs energy (with ΔG^0_{U1} = 9.9 kcal mol^{-1} and T_1 = 323.15 K) resulted also in similar ΔH_1 and ΔC_p as the ones obtained from direct analysis of MST1 inhibitory-SARAH thermal denaturation: 57 kcal mol^{-1} and 2 kcal mol^{-1} deg^{-1}, respectively (at 323.15 K).

Interestingly, at biologically relevant temperature (37 °C), the difference between the overall stability of the SARAH dimer (9.2 kcal mol^{-1}, which implies unfolding and dissociation) and its dissociation (8.62 ± 0.28 kcal mol^{-1}, the averaged value between CD and ITC) is only 0.58 ± 0.28 kcal mol^{-1}. This low difference would correspond to a low residual structure within the monomer upon dissociation. In the case of MST1 inhibitory-SARAH, ΔG^0_U is ∼11 kcal mol^{-1}, while the Gibbs energy corresponding to dissociation is 10.14 ± 0.54 kcal mol^{-1} (K_D is 0.1 ± 0.07 μM). The difference of 0.86 ± 0.54 kcal mol^{-1} represents the stability of the SARAH monomer within the inhibitory-SARAH construct after dissociation. Thus, the inhibitory domain does not influence significantly the stability of the SARAH domain within the monomer, but it stabilizes the dimer mainly by stabilizing the interface.

MST1 Inhibitory Domain Is an Intrinsically Disordered Region (IDR). It was previously shown that the inhibitory domain of MST1 contains a low percentage of secondary structure, and it is highly flexible.[29] Here, we tried to get more information about its structural and biophysical characteristics. Both MST1 inhibitory and inhibitory-SARAH were found to elute at more than double the expected molecular weight (data not shown).

The hydrodynamic radius (R_H) of MST1 inhibitory and MST1 inhibitory-SARAH was determined by DLS and compared with that of H-Ras, cytochrome *c*, and lysozyme under physiologic and denaturating conditions (Figure S8). Cytochrome, lysozyme, and Ras were used as references because they are well folded, compact, and almost spherical proteins with molecular weights (MWs) comparable to MST1 inhibitory. The results of the DLS experiments indicate that MST1 inhibitory has an extraordinary large R_H (3.08 nm). Although Ras (18.9 kDa), lysozyme (14.3 kDa), and cytochrome *c* (12.2 kDa) have larger MWs than MST1 inhibitory (11.8 kDa), they have smaller R_Hs under physiologic conditions (Figure S8). In fact, the R_H of MST1 inhibitory is rather comparable with that of lysozyme and cytochrome *c* under denaturating conditions (pH 2, 8 M urea). The dimeric complex MST1 inhibitory-SARAH has an extremely large R_H of 4.52 nm (corresponding to a volume 8 times larger than the other proteins analyzed here), although its MW is only 37.5 kDa.

Cross-linking experiments using DSG or EDC show that MST1 inhibitory does not oligomerize and that MST1 inhibitory-SARAH cross-links only as dimers (Figure S9a,c). Interestingly, the usage of the cross-linking compound EDC results in the formation of bands with smaller apparent MWs than un-cross-linked monomeric MST1 inhibitory and MST1 inhibitory-SARAH (Figure S9b,d). Similar observations were made in the case of intrinsically disordered proteins (IDPs) as a consequence of intramolecular cross-linking due to the conformational flexibility of the polypeptide chain.[53] The consequence of intramolecular cross-linking is that the polypeptide chain becomes incrementally more compact and cannot be unfolded completely by SDS. Therefore, intra-

molecular cross-linked proteins migrate on SDS gels faster than their un-cross-linked counterparts. In extreme cases, the scale of intramolecular cross-linking is so large that the polypeptide chains cannot be visualized anymore on SDS gels (Figure S9b,d).

As shown above (Figure S6a), the CD spectrum of the inhibitory domain shows no significant ellipticity change at 222 nm when heated, although it is important to mention that it goes from −3.3 mdeg at 10 °C to −5.4 mdeg at 80 °C. We also find a far-UV profile characteristic for random coil structure with a minimum at 200 nm (data not shown).

The low unfolding enthalpy that is obtained from the DSC thermogram (Figure 4) could represent the energetics of the few intramolecular interactions within a single or several small folded regions of MST1 Inhibitory. Upon heating, proteins with hydrophobic cores tend to aggregate. The degree of aggregation of proteins (hence their solubility) can be recorded by measuring their optical densities (ODs) at 350 nm (turbidity assay). The solubility of MST1 inhibitory was compared with that of four well-folded proteins (H-Ras, ovalbumin, lysozyme, and NORE1-C1-RBD). After being heated, the solutions of H-Ras, ovalbumin, lysozyme, and NORE1-C1-RBD became turbid and showed ODs of 0.28−1.51 (Figure 6). In contrast to the other proteins, the solution with MST1 inhibitory practically does not change its OD before (OD = 0.0067) and after (OD = 0.0148) heating to 95 °C, indicating that MST1 inhibitory does not aggregate upon heating and thus remains well soluble.

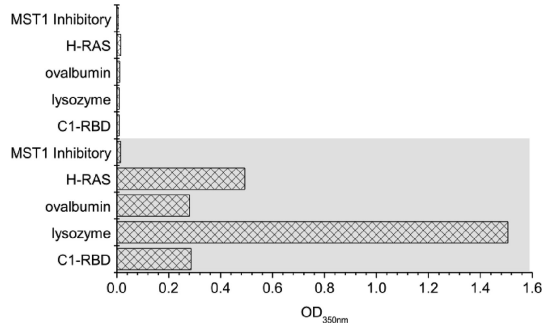

Figure 6. Turbidity assays for MST1 inhibitory, H-RAS (1−166), ovalbumin, lysozyme, and NORE1-C1-RBD. The ODs (at 350 nm) of the protein solutions were measured first at 20 °C and after being heated to 95 °C for 10 min and cooled rapidly to 20 °C (highlighted by a gray background).

Radivojac et al.[46] classify amino acids in respect to their abundance in ordered and disordered proteins as neutral (A and G), order promoting (C, W, Y, I, F, V, L, H, T, and N), and disorder promoting (D, M, K, R, S, Q, P, and E). According to this classification, only 23.5% of the amino acids of MST1 inhibitory are order promoting, while 55% are disorder promoting (the rest of the amino acids are neutral with respect to folding). MST1 inhibitory has with its 71.6% (31.4% of them are charged amino acids!) a very high content of amino acids with a negative hydropathy index. It is important to note that the domain is composed of 20% negatively charged residues (E and D). Consequently, it has a very low pI (4.5) and a very high net charge at neutral pH.

DISCUSSION

Self-association of MST1 and the resulting intermolecular autophosphorylation are important for its biological activity.[1,11,28,30,31] The extreme C-terminal domain, known as SARAH domain, seems to be essential for driving homo-oligomerization of MST1 and of related proteins. SARAH is also important for interactions between several partners containing this domain, leading to different responses like apoptosis and cell growth restriction.

It was found that MST1 SARAH forms an antiparallel helical dimer and that the dimer seems to be very stable with an expected K_D in the nanomolar range.[29]

Here we show that MST1 SARAH monomer is stable only in the dimeric state and that the equilibrium homo/heterodimer could involve a partially disordered monomeric intermediate. It is possible that not only the high degree of reversibility but also a residual structure within the monomer (although having low stability) might have an important role for the chain exchange in the equilibrium between homodimeric and heterodimeric state. In addition, we have analyzed the biophysical features and the contribution of the inhibitory domain to the overall SARAH stability and affinity.

MST1 SARAH thermal unfolding was found to be concentration dependent. This was not unexpected, as it was found to form dimers that could dissociate during denaturation. The increase in T_m with the concentration was the first indication that the protein underwent dissociation during the transition. The theoretical ΔH_{vH} obtained from eq 2 for a dimer−monomer equilibrium, the ΔH_{vH} determined from linear dependency of T_m on natural logarithm of concentration (or ΔH_{conc}), and the calorimetric enthalpy, ΔH_{cal}, obtained after normalizing the thermogram to the protein concentration expressed as dimers were in good agreement, with a slightly larger ΔH_{conc}. This and the linear dependency of inverse of T_p with the natural logarithm of the total protein concentration indicate that the unfolding and the dissociation occur simultaneously, a conclusion supported further by CD measurements. The model of dimer−monomer equilibrium finds the strongest support by our experimental data, the other two models (trimer-to-monomer or tetramer-to-monomer equilibrium) being disfavored, in particular as there is a large difference in ΔH_{conc} in comparison to the other two enthalpies. Also, the good agreement between calculated ΔG^0_U at different concentrations for a particular temperature in the transition region (Figure 5) supports this model.

Different ΔH_{conc} compared to the other two ΔH values is expected for non-two-state equilibrium implying intermediate states or/and characterized by incomplete dissociation, the transition being controlled by the unfolding constant.[36] This is observed for both DSC and CD measurements, but interestingly, the ΔH_{conc} value from CD is very similar to ΔH_{cal} and with ΔH_{vH} (calculated with eq 2) from DSC (77, 76, and 70 kcal mol^{-1}, respectively). The presence of two sequential transitions could be associated with different steps in the overall process. This could be due to two thermodynamic domains of SARAH having different stabilities. Another possible explanation may be related to the linear increase of C_p with temperature in the pretransition region (Figure S1). It is possible that this effect is due to real conformational changes that should not be eliminated from the analysis of the thermograms. The difference between ΔH_{conc} and the other ΔH values, as mentioned above, could then result from changes in the tertiary structure in the course of this pre-transition region that are not detected by far-UV CD (one should consider the fact that the pre-transition was ignored when determining ΔH_{cal} and theoretical ΔH_{vH}, as well as when

deconvoluting the thermograms). In fact, there are several reports showing that different coiled coil domains undergo several conformational changes before the main cooperative transition: fraying of ends, coiled coil α-helix (which has a rise of 5.15 Å/turn) to a canonical straight α-helix transition (with a rise of 5.4 Å/turn), or repacking of coiled coil.[41,44]

The dissociation of MST1 SARAH probed by CD and ITC shows some important features. The K_D is in low micromolar range (an average of 1 μM) at physiological temperature. Probably one of the most interesting features is that there is only a small difference (0.58 ± 0.28 kcal mol^{-1}) between the free energy measured by dilution experiments (ITC and CD) and the one obtained from thermal denaturation, at physiological temperature. This implies that the dissociation of the dimer at 37 °C triggers also partial unfolding of the monomer, and the folding is thus induced by association. There are two conclusions that can be extracted from this result. On one hand, this low difference (0.58 ± 0.28 kcal mol^{-1} from a total protein stability of 9.2 kcal mol^{-1} at 37 °C) signifies that the dissociation does not trigger the complete unfolding of the domain. On the other hand, the low stability of this intermediate state between the folded dimer and the completely unfolded monomer would make it almost undetectable in the denaturation transition. This is better understood from Figure 7, where the protein concentration

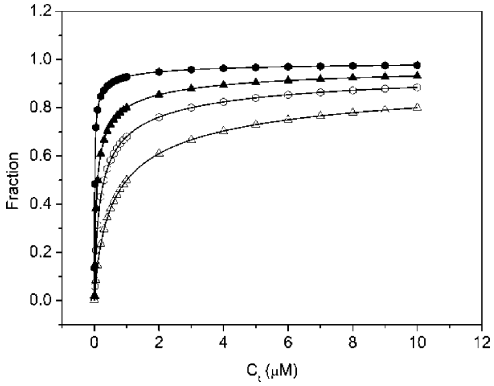

Figure 7. Fraction of folded-associated protein (● and ▲, measured from thermal denaturation) and associated protein (○ and △, measured from dilution experiments) for MST1 SARAH (▲ and △) and MST1 inhibitory-SARAH (● and ○).

dependency of the unfolded (plus dissociated) fraction (calculated from K_U at 37 °C) is compared to that of the fraction of the dissociated protein (calculated from the averaged K_D of 1 μM at 37 °C).

As SARAH domain in isolation could behave differently with respect to the peptide extended to the N-terminal end, the influence of the inhibitory domain (the adjacent 100 amino acids) was investigated. Indeed, it was noticed that SARAH domain displays a higher thermal stability. More, the lack of measurable signal in ITC experiments suggested that the affinity of the longer construct is higher than that of the isolated SARAH domain or/and that the enthalpy of dissociation/unfolding is too low to be detected. Indeed, a 10 times lower K_D was obtained from CD dilutions. Nevertheless, the thermal unfolding is still concentration dependent and can be fitted to a two-state with dissociation model. As the inhibitory domain is almost completely unfolded when the transition of SARAH denaturation starts, we propose that the stabilization observed is mainly due to residues of inhibitory domain contacting SARAH.

The inhibitory domain has almost no influence on the stability of the SARAH monomer, the difference between the unfolding (plus dissociation) and the dissociation Gibbs energy being still low (0.86 ± 0.54 kcal mol^{-1}). As can been seen in Figure 7, the fractions of folded/associated dimers have similar trends as those of SARAH domain alone, although the saturation is reached at lower concentration (as expected, due to the lower K_D). We suggest that the SARAH domain undergoes at least partial unfolding even at physiologically relevant temperatures and that the folded monomer is low populated.

The characterization of the MST1 inhibitory domain by CD spectroscopy, cross-linking, DLS, and turbidity assays strongly indicates that it is an intrinsically disordered region (IDR). The unfolding enthalpy (ΔH) of MST1 inhibitory of 8 kcal mol^{-1} measured by DSC (Figure 4) is, in comparison to folded proteins, very small. Assuming an average MW of 115 Da for an amino acid, ΔH for MST1 Inhibitory is only 0.078 kcal mol^{-1} residue^{-1}. Folded proteins have roughly 12 times larger ΔH values. For example myoglobin, lysozyme, and ubiquitin have ΔH of 0.813, 1.028, and 0.956 kcal mol^{-1} residue^{-1}, respectively.[47] Moreover, the domain is not significantly stabilized by dimerization because ΔH of MST1 Inhibitory-SARAH is with its 46 kcal mol^{-1} only slightly larger than the sum of ΔH of MST1-SARAH and MST1 inhibitory (42 kcal mol^{-1}) measured separately. This means that the domain remains disordered not only as a single domain but also as part of the larger construct and within the dimeric complex. The very small ΔH of MST1 inhibitory unfolding and its resistance to heat-mediated aggregation (Figure 6) indicate that there is no hydrophobic core with significant extension. Most of the IDPs investigated by DSC up to now appeared to display no cooperative transition, but either no change of the heat capacity or a gradual transition.[48−50] Nevertheless, it should be emphasized that there are not as many DSC investigations of IDPs as there are for folded proteins. Thus, there is not so much knowledge about unfolding of the different types of IDPs. Our result indicates that the inhibitory domain might contain small local clusters of interactions.

Lack of typical absorption bands of secondary structural elements and no cooperative unfolding transition upon increase of temperature in the CD spectra (Figure S6a) indicate that MST1 Inhibitory contains a low percentage of secondary structural elements. Interestingly, one can observe a slight increase (and not a decrease, as in the case of typical unfolding) in the absolute value at 222 nm. More, one would expect that the unfolding seen in the DSC thermogram would have a correspondence in the far-UV CD. This discrepancy is discussed in the following paragraph.

The inhibitory domain was previously shown to contain 20% α-helix and 3% β-sheet.[29] Still, this percentage does not apply to single molecules, as the far-UV CD spectrum provides information about the ensemble of conformations.[51] The proteins do not adopt a defined structure, and secondary structure elements can form transiently. Nevertheless, considering that this percentage is real, we should indeed be able to follow the unfolding at 222 nm. The fact that we do not observe this seems to have a reasonable explanation. The denaturation of IDPs should be treated in a different manner than the one of the folded proteins. Temperature-induced structural changes were investigated by far-UV CD for many

IDPs, and in most of the cases, no classical unfolding trend of the secondary elements was observed (refs 50 and 51 and references therein). On the contrary, the change of spectra was in the opposite direction, a gain in negative ellipticity around 222 nm and a loss of negative ellipticity at 200 nm. This was interpreted as formation of α-helices and to a minor extent as a loss of the polyproline II (PPII) structure. The difficulty in interpreting the changes observed by CD comes from the fact that the spectroscopic contributions coming from structural changes in different fragments can cancel each other's signal changes. Recently, it was proposed that the effect observed by CD in case of IDPs comes from the unfolding of the PPII helices, as the NMR chemical shifts showed loss in the α-helical content.[52] More, Uversky[53] has established two categories of the IDPs, i.e., coil-like (having ~30% PPII) and premolten globule (PMG)-like (with ~10% PPII) based on the different molar ellipticities at 200 and 222 nm and on the correlation between the hydrodynamic volume and the number of residues.

Based on our data, the inhibitory domain of MST1 would fall closer to the coil-like type, although the hydrodynamic volume is only 5−6 times larger (and not 12, as proposed in case of coil-like unstructured proteins; see ref 53) than the one corresponding to a compact folded protein with same MW. This result indicates that the inhibitory domain is disordered but not completely unstructured. Our CD measurements also indicate a slight gain in ellipticity at 222 nm and a loss at 200 nm (data not shown) at high temperatures, typical to the ones seen before. Taking into consideration the previous observations, we suggest that the unfolding of α-helices is masked by the loss of the PPII content which has an opposite effect. Thus, the far-UV CD reports on the unfolding of the local secondary structure of the domain, but there is an overlap between α-helix melting and PPII unfolding, having opposite effects on the CD spectrum. It remains to be established how these conformational changes correlate with the transition observed with DSC. It is possible that this domain behaves as an atypical IDP.

The low hydrophobicity and the high net charge of MST1 inhibitory implicate the existence of a relatively large hydration shell and explain, along with the structural flexibility, its extraordinary large volume. Flexible protein segments are sterically better accessible for proteases and are proteolyzed more efficiently than folded ones.[54] Additionally, a computer-based analysis of 280 caspase substrates revealed that 78% of caspase cleavage sites are located within random coils.[55] Moreover, the majority of caspase cleavage sites are found in the close vicinity of so-called PEST-rich protein regions, which are reported to be unstructured.[56] PEST-rich regions contain a disproportionately high number of P, E/D, S, T, N, and Q residues, and MST1 inhibitory is composed of 48% of these residues. Taking into consideration that there are two caspase recognition motives within the inhibitory domain (DEMD^{326}S and TMTD^{349}S) and that the full activation of MST1 during apoptosis requires a caspase-mediated removal of the kinase domain from the rest of the protein,[57] the lack of folding may be important for the efficient proteolysis of MST1 by caspases.

In conclusion, we have shown that the dimerization domain of MST1 kinase is partially unstructured in the monomeric state and that it undergoes association-induced folding. Many coiled coils peptides follow this mechanism of interaction, but this is not a general rule.[58] Coupling of folding and binding is often encountered in biological processes, especially in signal transduction, cell cycle control, and transcription.[59−61] It has an important role in regulation of the binding thermodynamics[62,63] and the rates of macromolecular associations.[64] We also show that the inhibitory domain is an intrinsically disordered region (IDR) both as a single domain and in the inhibitory-SARAH construct, with implications in caspase cleavage and kinase autophosphorylation. We propose that MST1 SARAH monomer also behaves as a partially disordered region upon dimer dissociation. Intrinsic disorder was found to occur very often in the case of proteins binding to more than one target (extensive protein interaction networks), called hub proteins.[65] Thus, the structural plasticity facilitates the protein to adopt different conformations, depending on the binding partner. As the SARAH domain is responsible for homodimerization but also for heterointeractions with other proteins (such as the Rassf proteins), it becomes clear the necessity for dissociation-induced unfolding when switching from one complex to another. The high degree of reversibility, but also a residual secondary structure within the monomer (having a stability of 0.86 ± 0.54 kcal mol^{-1}) that would be stabilized in the bound state (inherent-structure mechanism[65−69]), could increase the association rates, reduce the entropic penalty, and increase the overall affinity. Further investigation of the transition between the homodimer and the complexes with other binding partners will bring important insights into the mechanism of Ras-mediated apoptosis.

■ ASSOCIATED CONTENT

Supporting Information

Tables S1 and S2 and Figures S1−S9. This material is available free of charge via the Internet at http://pubs.acs.org.

■ AUTHOR INFORMATION

Corresponding Author

*Tel: +49 (0)234 3224173; Fax: +49 (0)234 3214785; e-mail chr.herrmann@rub.de.

Author Contributions

†These authors contributed equally.

Funding

This work was financially supported by Deutsche Forschungsgemeinschaft SFB642 and the Marie Curie EU Project INTCHEM (MEST-CT-2005-020681; fellowship for D.C.A.).

■ REFERENCES

(1) Graves, J. D., Draves, K. E., Gotoh, Y., Krebs, E. G., and Clark, E. A. (2001) Both phosphorylation and caspase-mediated cleavage contribute to regulation of the Ste20-like protein kinase Mst1 during CD95/FAS-induced apoptosis. *J. Biol. Chem. 276*, 14909−14915.

(2) Ura, S., Masuyama, N., Graves, J. D., and Gotoh, Y. (2001) MST1-JNK promotes apoptosis via caspase-dependent and independent pathways. *Genes Cells 6*, 519−530.

(3) Ura, S., Nishina, H., Gotoh, Y., and Katada, T. (2007) Activation of the c-Jun N-terminal kinase pathway by MST1 is essential and sufficient for the induction of chromatin condensation during apoptosis. *Mol. Cell. Biol. 27*, 5514−5522.

(4) Lin, J. L., Chen, H. C., Fang, H. I., Robinson, D., Kung, H. J., and Shih, H. M. (2001) MST4, a new Ste20-related kinase that mediates cell growth and transformation via modulating ERK pathway. *Oncogene 20*, 6559−6569.

(5) Qian, Z., Lin, C., Espinosa, R., LeBeau, M., and Rosner, M. R. (2001) Cloning and characterization of MST4, a novel Ste20-like kinase. *J. Biol. Chem. 276*, 22439−22445.

(6) O'Neill, E., Rushworth, L., Baccarini, M., and Kolch, W. (2004) Role of the Kinase MST2 in Suppression of Apoptosis by the Proto-Oncogene Product Raf-1. *Science 306*, 2267−2270.

(7) O'Neill, E., and Kolch, W. (2005) Taming the Hippo: Raf-1 controls apoptosis by suppressing MST2/Hippo. *Cell Cycle 4*, 365–367.
(8) O'Neill, E. E., Matallamus, D., and Kolch, W. (2005) Mammalian Sterile 20-Like Kinases in Tumor Suppression: An Emerging Pathway. *Cancer Res. 65*, 5485–5487.
(9) Lin, Y., Khokhlatchev, A., Figeys, D., and Avruch, J. (2002) Death-associated Protein 4 Binds MST1 and Augments MST1-induced Apoptosis. *J. Biol. Chem. 277*, 47991–48001.
(10) Taylor, L. K., Wang, H. C., and Erikson, R. L. (1996) Newly identified stress-responsive protein kinases, Krs-1 and Krs-2. *Proc. Natl. Acad. Sci. U. S. A. 93*, 10099–10104.
(11) Creasy, C. L., and Chernoff, J. (1995) Cloning and characterization of a human protein kinase with homology to Ste20. *J. Biol. Chem. 270*, 21695–21700.
(12) Watabe, M., Kakeya, H., and Osada, H. (1999) Requirement of protein kinase (Krs/MST) activation for MT-21-induced apoptosis. *Oncogene 18*, 5211–5220.
(13) Watabe, M., Kakeya, H., Onose, R., and Osada, H. (2000) Activation of MST/Krs and c-Jun N-terminal kinases by different signaling pathways during cytotrienin A-induced apoptosis. *J. Biol. Chem. 275*, 8766–8771.
(14) De Souza, P. M., and Lindsay, M. A. (2004) Mammalian Sterile20-like kinase 1 and the regulation of apoptosis. *Biochem. Soc. Trans. 32*, 485–488.
(15) Fernando, P., Kelly, J. F., Balazsi, K. R., Slack, S., and Megeney, L. A. (2002) Caspase 3 activity is required for skeletal muscle differentiation. *Proc. Natl. Acad. Sci. U. S. A. 99*, 11025–11030.
(16) Yamamoto, S., Yang, G., Zablocki, D., Liu, J., Hong, C., Kim, S. J., Soler, S., Odashima, M., Thaisz, J., Yehia, G., Molina, C. A., Yatani, A., Vatner, S. F., and Sadoshima, J. (2003) Activation of Mst1 causes dilated cardiomyopathy by stimulating apoptosis without compensatory ventricular myocyte hypertrophy. *J. Clin. Invest. 111*, 1463–1474.
(17) Lian, J. P., Toker, A., and Badwey, J. A. (2001) Phosphorylation of the activation loop of gamma p21-activated kinase (gamma-Pak) and related kinases (MSTs) in normal and stressed neutrophils. *J. Immunol. 166*, 6349–6357.
(18) De Souza, P. M., Kankaanranta, H., Michael, A., Barnes, P. J., Giembycz, M. A., and Lindsay, M. A. (2002) Caspase-catalyzed cleavage and activation of Mst1 correlates with eosinophil but not neutrophil apoptosis. *Blood 99*, 3432–3438.
(19) Ono, H., Ichiki, T., Ohtsubo, H., Fukuyama, K., Imayama, I., Hashiguchi, Y., Sadoshima, J., and Sunagawa, K. (2005) Critical role of Mst1 in vascular remodeling after injury. *Arterioscler. Thromb. Vasc. Biol. 25*, 1871–1876.
(20) Seidel, C., Schagdarsurengin, U., Blumke, K., Wurl, P., Pfeifer, G. P., Hauptmann, S., Taubert, H., and Dammann, R. (2007) Frequent hypermethylation of MST1 and MST2 in soft tissue sarcoma. *Mol. Carcinog. 46*, 865–871.
(21) Chan, E. H., Nousiainen, M., Chalamalasetty, R. B., Schafer, A., Nigg, E. A., and Sillje, H. H. (2005) The Ste20-like kinase Mst2 activates the human large tumor suppressor kinase Lats1. *Oncogene 24*, 2076–2086.
(22) Cheung, W. L., Ajiro, K., Samejima, K., Kloc, M., Cheung, P., Mizzen, C. A., Beeser, A., Etkin, L. D., Chernoff, J., Earnshaw, W. C., and Allis, C. D. (2003) Apoptotic phosphorylation of histone H2B is mediated by mammalian sterile twenty kinase. *Cell 113*, 507–517.
(23) Ahn, S. H., Cheung, W. L., Hsu, J. Y., Diaz, R. L., Smith, M. M., and Allis, C. D. (2005) Sterile 20 kinase phosphorylates histone H2B at serine 10 during hydrogen peroxide-induced apoptosis in S. cerevisiae. *Cell 120*, 25–36.
(24) Teraishi, F., Guo, W., Zhang, L., Dong, F., Davis, J. J., Sasazuki, T., Shirasawa, S., Liu, J., and Fang, B. (2006) Activation of sterile20-like kinase 1 in proteasome inhibitor bortezomib-induced apoptosis in oncogenic K-ras-transformed cells. *Cancer Res. 66*, 6072–6079.
(25) Lehtinen, M. K., Yuan, Z., Boag, P. R., Yang, Y., Villen, J., Becker, E. B., DiBacco, S., de la Iglesia, N., Gygi, S., Blackwell, T. K., and Bonni, A. (2006) A conserved MST-FOXO signaling pathway mediates oxidative-stress responses and extends life span. *Cell 125*, 987–1001.
(26) Cinar, B., Fang, P.-K., Lutchman, M., Di Vizio, D., Adam, R. M., Yelick, P. C., and Freeman, M. R. (2007) The pro-apoptotic kinase Mst1 and its caspase cleavage products are direct inhibitors of Akt1. *EMBO J. 26*, 4523–4534.
(27) Jang, S. W., Yang, S.-J., Srinivasan, S., and Ye, K. (2007) Akt phosphorylates Mst1 and prevents its proteolytic activation, blocking FOXO3 phosphorylation and nuclear translocation. *J. Biol. Chem. 282*, 30836–30844.
(28) Glantschnig, H., Rodan, G. A., and Reszka, A. A. (2002) Mapping of MST1 kinase sites of phosphorylation. Activation and autophosphorylation. *J. Biol. Chem. 277*, 42987–42996.
(29) Hwang, E., Ryu, K. S., Paakkonen, K., Guntert, P., Cheong, H. K., Lim, D. S., Lee, J. O., Jeon, Y. H., and Cheong, C. (2007) Structural insight into dimeric interaction interaction of the SARAH domains from Mst1 and RASSF family proteins in the apoptosis pathway. *Proc. Natl. Acad. Sci. U. S. A. 104*, 9236–9241.
(30) Anand, R., Kim, A. Y., Brent, M., and Marmorstein, R. (2008) Biochemical Analysis of MST1 Kinase: Elucidation of a C-Terminal Regulatory Region. *Biochemistry 47*, 6719–6726.
(31) Creasy, C. L., Ambrose, D. M., and Chernoff, J. (1996) The Ste20-like protein kinase, Mst1, dimerizes and contains an inhibitory domain. *J. Biol. Chem. 271*, 21049–21053.
(32) Khokhlatchev, A., Rabizadeh, S., Xavier, R., Nedwidek, M., Chen, T., Zhang, X. F., Seed, B., and Avruch, J. (2002) Identification of a novel Ras-regulated proapoptotic pathway. *Curr. Biol. 12*, 253–265.
(33) Record, C. J., Chaikuad, A., Rellos, P., Das, S., Pike, A. C. W., Fedorov, O., Marsden, B. D., Knapp, S., and Lee, W. H. (2010) Structural Comparison of Human Mammalian Ste20-Like Kinases. *PLoS One 5*, e11905.
(34) Bradford, M. M. (1976) A Rapid and Sensitive Method for the Quantitation of Microgram Quantities of Protein Utilizing the Principle of Protein-Dye Binding. *Anal. Biochem. 72*, 248–254.
(35) Privalov, P. L., and Potekhin, S. A. (1986) Scanning microcalorimetry in studying temperature induced changes in proteins. *Methods Enzymol. 131*, 4–51.
(36) Lepock, J. R., Frey, H. E., and Hallewell, R. A. (1990) Contribution of Conformational Stability and Reversibility of Unfolding to the Increased Thermostability of Human and Bovine Superoxide Dismutase Mutated at Free Cysteines. *J. Biol. Chem. 265*, 21612–21618.
(37) Koppenol, S. (2008) *Physical Considerations in Protein and Peptide Stability* (McNally, E. J., and Hastedt, J. E., Eds.) pp 43–72, Informa Healthcare/USA, New York.
(38) Sturtevant, J. M. (1987) Biochemical Applications of Differential Scanning Calorimetry. *Annu. Rev. Phys. Chem. 38*, 463–488.
(39) Lassalle, M. W., Hinz, H.-J., Wenzel, H., Vlassi, M., Kokkinidis, M., and Cesareni, G. (1998) Dimer-to-Tetramer Transformation: Loop Excision Dramatically Alters Structure and Stability of the Rop four α-helix Bundle Protein. *J. Mol. Biol. 279*, 987–1000.
(40) Téllez-Sanz, R., Cesareo, E., Nuccetelli, M., Aguilera, A. M., Barón, C., Parker, L. J., Adams, J. J., Morton, C. J., Bello, M. L., Parker, M. W., and García-Fuentes, L. (2006) Calorimetric and structural studies of the nitric oxide carrier S-nitrosoglutathione bound to human glutathione transferase P1–1. *Protein Sci. 15*, 1093–1105.
(41) Greenfield, N. J., and Hitchcock-Degregori, S. E. (1993) Conformational intermediates in the folding of a coiled-coil model peptide of the N-terminus of tropomyosin and $\alpha\alpha$-tropomyosin. *Protein Sci. 2*, 1263–1273.
(42) Shriver, J. W., and Edmondson, S. P. (2009) Defining the Stability of Multimeric Proteins, in *Protein Structure, Stability, and Interactions* (Shriver, J. W., Ed.) pp 57–82, Humana Press/USA, New York.
(43) Greenfield, N. J. (2006) Using circular dichroism collected as a function of temperature to determine the thermodynamics of protein unfolding and binding interactions. *Nature Protocols 1*, 2527–2535.

(44) Dragan, A. I., and Privalov, P. L. (2002) Unfolding of a Leucine zipper is not a Simple Two-state Transition. *J. Mol. Biol. 321*, 891−908.
(45) Bowie, J. U., and Sauer, R. T. (1989) Equilibrium Dissociation and Unfolding of the Arc Repressor Dimer. *Biochemistry 28*, 7139−7143.
(46) Radivojac, P., Iakoucheva, L. M., Oldfield, C. J., Obradovic, Z., Uversky, V. N., and Dunker, A. K. (2007) Intrinsic disorder and functional proteomics. *Biophys. J. 92*, 1439−1456.
(47) Privalov, P. L., and Dragan, A. I. (2007) Microcalorimetry of biological macromolecules. *Biophys. Chem. 126*, 16−24.
(48) Mendoza, C., Figueirido, F., and Tasayco, M. L. (2003) DSC Studies of a Family of Natively Disordered Fragments from *Escherichia coli* Thioredoxin: Surface Burial in Intrinsic Coils. *Biochemistry 42*, 3349−3358.
(49) Ishihima, J., Nagasaki, N., Maeshima, M., and Miyano, M. (2007) RVCaB, a Calcium-binding Protein in Radish Vacuoles, is Predominantly an Unstructured Protein with a Polyproline Type II Helix. *J. Biochem. 142*, 201−211.
(50) Wang, X., Zhang, S., Zhang, J., Huang, X., Xu, C., Wang, W., Liu, Z., Wu, J., and Shi, Y. (2010) A Large Intrinsically Disordered Region in SKIP and Its Disorder-Order Transition Induced by PPIL1 Binding Revealed by NMR. *J. Biol. Chem. 285*, 4951−4963.
(51) http://www.disprot.org/data/detection/NatDisPro.pdf.
(52) Kjaergaard, M., Nørholm, A.-B., Hendus-Altenburger, R., Pedersen, S. F., Poulsen, F. M., and Kragelund, B. B. (2010) Temperature-dependent structural changes in intrinsically disordered proteins: Formation of α-helices or loss of polyproline II? *Protein Sci. 19*, 1555−1564.
(53) Uversky, V. N. (2002) Natively unfolded proteins: A point where biology waits for physics. *Protein Sci. 11*, 739−756.
(54) Tsai, C.-J., Polverino de Laureto, P., Fontana, A., and Nussinov, R. (2002) Comparison of protein fragments identified by limited proteolysis and by computational cutting of proteins. *Protein Sci. 11*, 1753−1770.
(55) Garay-Malpartida, H. M., Occhiucci, J. M., Alves, J., and Belizario, J. E. (2005) CaSPredictor: a new computer-based tool for caspase substrate prediction. *Bioinformatics 21*, 169−176.
(56) Tompa, P. (2002) Intrinsically unstructured proteins. *Trends Biochem. Sci. 27*, 527−533.
(57) Graves, J. D., Gotoh, Y., Draves, K. E., Ambrose, D., Han, D. K. M., Wright, M., Chernoff, J., Clark, E. A., and Krebs, E. G. (1998) Caspase-mediated activation and induction of apoptosis by the mammalian Ste20-like kinase Mst1. *EMBO J. 17*, 2224−2234.
(58) Gnanapragasam, M. N., Scarsdale, J. N., Amaya, M. L., Webb, H. D., Desai, M. A., Walavalkar, N. M., Wang, S. Z., Zhu, S. Z., Ginder, G. D., and Williams, D. C. Jr. (2011) p66α-MBD2 coiled-coil interaction and recruitment of Mi-2 are critical for globin gene silencing by the MBD2-NuRD complex. *Proc. Natl. Acad. Sci. U. S. A. 108*, 7487−7492.
(59) Iakoucheva, L. M., Brown, C. J., Lawson, J. D., Obradović, Z., and Dunker, A. K. (2002) Intrinsic Disorder in Cell-signaling and Cancer-associated Protein. *J. Mol. Biol. 323*, 573−584.
(60) Galea, C. A., Wang, Y., Sivakolundu, S. G., and Kriwacki, R. W. (2008) Regulation of Cell Division by Intrinsically Unstructured Proteins: Intrinsic Flexibility, Modularity and Signaling Conduits. *Biochemistry 47*, 7598−7609.
(61) Uversky, V. N., Oldfield, C. J., and Dunker, A. K. (2005) Showing your ID: intrinsic disorder as an ID for recognition, regulation and cell signaling. *J. Mol. Recognit. 18*, 343−384.
(62) Demchenko, A. P. (2001) Recognition between flexible protein molecules: induced and assisted folding. *J. Mol. Recognit. 14*, 42−61.
(63) Dyson, H. J., and Wright, P. E. (2005) Intrinsically unstructured proteins and their functions. *Nat. Rev. Mol. Cell Biol. 6*, 197−208.
(64) Shoemaker, B. A., Portman, J. J., and Wolynes, P. G. (2000) Speeding molecular recognition by using the folding funnel: the fly-casting mechanism. *Proc. Natl. Acad. Sci. U. S. A. 97*, 8868−8873.
(65) Singh, G. P., Ganapathi, M., and Dash, D. (2007) Role of intrinsic disorder in transient interactions of hub proteins. *Proteins: Struct., Funct., Bioinf. 66*, 761−765.
(66) Oldfield, C. J., Cheng, Y., Cortese, M. S., Romero, P., Uversky, V. N., and Dunker, A. K. (2005) Coupled folding and binding with alpha-helix-forming molecular recognition elements. *Biochemistry 44*, 12454−12470.
(67) Miller, M. (2009) The Importance of Being Flexible. The Case of Basic Region Leucine Zipper Transcriptional Regulators. *Curr. Protein Pept. Sci. 10*, 244−269.
(68) Myers, J. K., and Oas, T. G. (1999) Reinterpretation of GCN4-p1 Folding Kinetics: Partial Helix Formation Precedes Dimerization in Coiled Coil Folding. *J. Mol. Biol. 289*, 205−209.
(69) Zitzewitz, J. A., Ibarra-Molero, B., Fishel, D. R., Terrry, K. L., and Matthews, C. R. (2000) Preformed Secondary Structure Drives the Association Reaction of GCN4-p1, a Model Coiled-coil System. *J. Mol. Biol. 296*, 1105−1116.
(70) Wilkins, D. K., Grimshaw, S. B., Receveur, V., Dobson, C. M., Jones, J. A., and Smith, L. J. (1999) Hydrodynamic radii of native and denatured proteins measured by pulse field gradient NMR techniques. *Biochemistry 38*, 16424−16431.